

Detecting AI-Generated Forgeries via Iterative Manifold Deviation Amplification

Jiangling Zhang¹ Shuxuan Gao¹ Bofan Liu¹ Siqiang Feng¹
 Jirui Huang¹ Yaxiong Chen^{1*} Ziyu Chen¹
¹Wuhan University of Technology

Abstract

The proliferation of highly realistic AI-generated images poses critical challenges for digital forensics, demanding precise pixel-level localization of manipulated regions. Existing methods predominantly learn discriminative patterns of specific forgeries, struggling with novel manipulations as editing techniques evolve. We propose the **Iterative Forgery Amplifier Network (IFA-Net)**, which shifts from learning “what is fake” to modeling “what is real”. Grounded in the principle that all manipulations deviate from the natural image manifold, IFA-Net leverages a frozen Masked Autoencoder (MAE) pretrained on real images as a universal realness prior. Our framework operates through a two-stage closed-loop process: an initial **Dual-Stream Segmentation Network (DSSN)** fuses the original image with MAE reconstruction residuals for coarse localization, then a **Task-Adaptive Prompt Injection (TAPI)** module converts this coarse prediction into guiding prompts that steer the MAE decoder to amplify reconstruction failures in suspicious regions, enabling precise refinement. Extensive experiments on four diffusion-based inpainting benchmarks show that IFA-Net achieves an average improvement of 6.5% in IoU and 8.1% in F1-score over the second-best method, while demonstrating strong generalization to traditional manipulation types.

1. Introduction

The rapid evolution of generative models—particularly the rise of diffusion-based approaches [26, 30, 33, 36]—has fundamentally reshaped the landscape of image synthesis. Modern diffusion models can now produce visuals that are nearly indistinguishable from genuine photographs, blurring the boundary between creation and deception. While these advances enable unprecedented creative applications, they also introduce critical challenges for digital forensics. As manipulated images proliferate across online platforms, reliable pixel-level localization becomes essential. Beyond

*Corresponding author: yaxiong.chen@whut.edu.cn

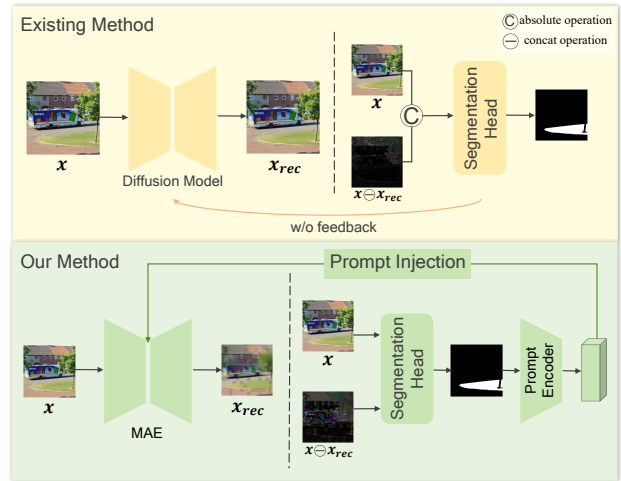


Figure 1. Conceptual comparison of our IFA-Net against existing methods. Existing methods often leverage Diffusion Models for reconstruction in a single-pass, open-loop process that lacks task-adaptive guidance. Our method is grounded in a different prior: a Masked Autoencoder (MAE) pretrained on real images. We introduce a two-stage, closed-loop framework where the coarse prediction from Stage 1 guides a second, targeted reconstruction in Stage 2 for significant anomaly amplification.

simply verifying authenticity, localization provides precise regions of manipulation, offering interpretable and actionable forensic evidence.

Despite significant advances, existing research still faces substantial limitations. Early forensic methods that relied on handcrafted cues—such as sensor noise or frequency inconsistencies [7]—collapse when confronted with modern generative pipelines, including subject-driven editing paradigms like DreamBooth [35]. Deep learning approaches improve robustness but often at the cost of architectural complexity. For instance, TruFor [13] integrates RGB and noise residuals through a transformer to detect anomalies; HiFi-Net [14] employs a multi-branch structure for fine-grained classification and localization; Diff-Forensics [42] leverages diffusion priors in a two-stage design; and UnionFormer [19] fuses object-level context with

multi-view representations. Although these architectures achieve strong performance, they remain heavy and tightly coupled to specific training distributions, resulting in poor generalization to unseen diffusion models. This persistent tension between specialization and generalization forms a central bottleneck in modern forensic localization. Methods such as MVSS-Net [9] further highlight this trend, excelling in known domains but struggling with unseen manipulation types. Fundamentally, these approaches learn discriminative patterns of known forgeries rather than modeling the intrinsic properties of authentic images, limiting their ability to detect novel manipulations.

To address these challenges, we introduce IFA-Net, a simple yet powerful framework grounded in the assumption that even the most realistic forgeries inevitably deviate from the natural image manifold. Rather than relying on a monolithic detector, Iterative Forgery Amplifier Network (IFA-Net) decomposes the problem into two complementary stages. In the first stage, a frozen Masked Autoencoder (MAE) pretrained on large-scale natural images acts as a universal artifact amplifier. Its reconstruction process naturally magnifies subtle inconsistencies in manipulated regions, transforming weak and heterogeneous traces into stronger and more coherent signals. In the second stage, a lightweight dual-stream segmentation network jointly analyzes the original and amplified representations. These two streams are bridged through a task-adaptive prior injection (TAPI) module, which dynamically injects the amplified priors into the segmentation process, enabling precise localization with minimal computational overhead.

Extensive experiments on multiple diffusion-based forgery benchmarks demonstrate that IFA-Net achieves consistent state-of-the-art localization accuracy and robust generalization to unseen generators. Our findings reveal that coupling a frozen universal prior with task-adaptive injection effectively bridges the long-standing gap between simplicity and generalization in image forgery localization.

Our main contributions are summarized as follows:

- Realness-driven detection paradigm: We model authenticity rather than memorizing forgery patterns, using a frozen MAE pretrained on natural images as a universal realness prior to detect manipulations through their deviations from the natural image manifold.
- Closed-loop amplification framework: We introduce a two-stage architecture where the Task-Adaptive Prior Injection (TAPI) module creates a feedback loop, converting coarse predictions into prompts that guide reconstruction to progressively amplify weak forgery signals.
- State-of-the-art with strong generalization: IFA-Net achieves superior performance on diffusion-based benchmarks, and demonstrates robust cross-dataset generalization to unseen generators and traditional tampering meth-

ods.

2. Related Work

2.1. Generated Image Detection

With the rapid advancement of diffusion models, synthetic images have become nearly indistinguishable from real ones, posing unprecedented challenges to visual forensics. This evolution marks a paradigm shift from artifact-based discrimination toward generative-aware forensic modeling. Early studies primarily focused on local artifact identification, while recent works have emphasized modeling global consistency and semantic coherence. TruFor [13] fused RGB texture and noise residuals to improve pixel-level localization, and watermark-based localization approaches such as EditGuard [43] further explored structural cues for tamper analysis.

In parallel, frequency-domain and multimodal cues have attracted increasing attention. Beyond visual cues, Zhou et al. [45] explored vision–language alignment to achieve multimodal consistency. However, existing detection paradigms remain largely discriminative and data-driven, relying on local texture or frequency biases within training distributions [46]. Proactive detection frameworks [1] highlight the need to anticipate unseen manipulations rather than fitting to known distributions, while MALP [2] extends this proactive view to localization by leveraging early anomaly cues. Universal detectors [29] similarly emphasize generator-agnostic modeling, reinforcing the importance of priors that generalize beyond training data. This motivates a shift toward reconstruction-based modeling that leverages the intrinsic discrepancy between real and synthetic image manifolds.

2.2. Detection Based on Reconstruction Error

These advances highlight the growing importance of generative priors and naturally motivate reconstruction-error-based detection. As diffusion models continue to improve in reconstruction fidelity, researchers have begun exploiting their inherent limitations in reproducing real images. Recent work explores contrastive reconstruction signals to strengthen discrepancy modeling, such as DRCT [5]. Inversion-based reconstruction methods have also shown promise, e.g., FakeInversion [4], where inversion trajectories expose generator-specific inconsistencies. Wang et al. [40] introduced a diffusion reconstruction-error framework capturing pixel-level discrepancies, while training-free reconstruction error detectors such as AER-OBLADE [32] and frequency-guided reconstruction methods such as FIRE [6] further demonstrate the generality of reconstruction-asymmetry cues. Building on latent reconstruction analysis, LARE² [24] demonstrated that latent-space reconstruction biases can further enhance generaliz-

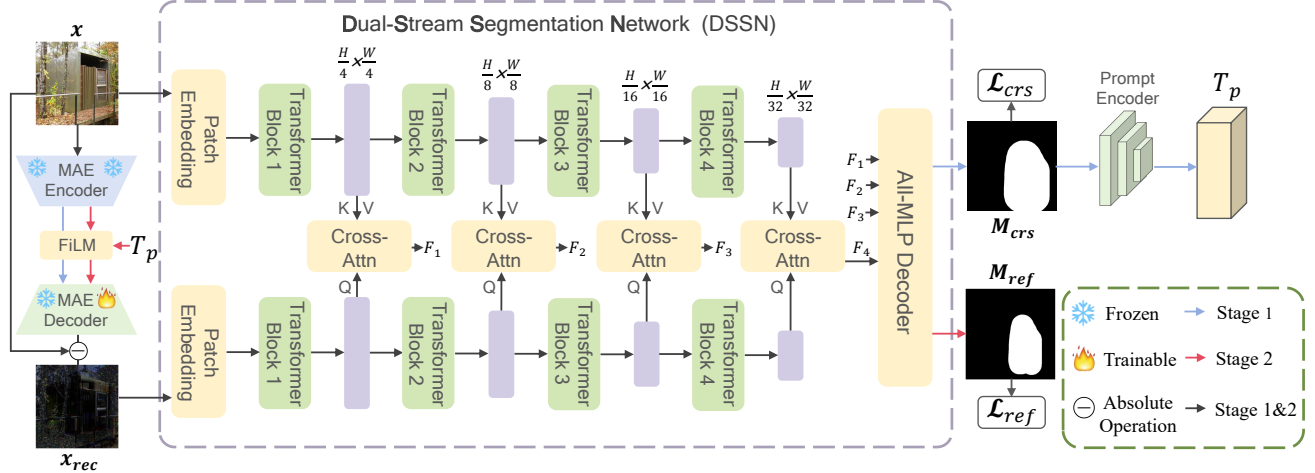


Figure 2. Overall architecture of IFA-Net. The framework operates in two stages while sharing the same Dual-Stream Segmentation Network (DSSN). Stage 1 (blue arrows): The input image x is processed by a fully frozen MAE (Encoder & Decoder) to produce an initial residual map x_{rec} . The DSSN then fuses x and x_{rec} to predict a coarse mask M_{crs} , supervised by \mathcal{L}_{crs} . Stage 2 (red arrows): The coarse mask M_{crs} is encoded into Task-Adaptive Prompts (T_p), which modulate features from the frozen MAE Encoder via a FILM layer. The modulated features are passed to a trainable MAE Decoder to generate an amplified residual map, which is then used by the shared DSSN to predict the final refined mask M_{ref} , supervised by \mathcal{L}_{ref} .

ability across unseen generators. Zhang et al. [44] proposed an INR-based preprocessing prior that stabilizes reconstruction and suppresses noise-sensitive residuals. Additional decomposition strategies have been discussed in prior work, but such approaches remain limited in their adaptability to diverse manipulation types.

Nevertheless, most reconstruction-based methods employ static generative priors that operate independently of the detection task, lacking adaptive feedback or semantic modulation [18, 22]. As a result, artifact amplification is unguided and reconstruction often emphasizes noise rather than task-relevant cues. To address these limitations, IFA-Net introduces a generative–discriminative collaborative framework that enables the reconstruction prior to be dynamically guided by the detection objective. By treating the pretrained MAE as a universal realness prior, IFA-Net encourages the model to learn which regions conform to the natural image manifold instead of merely memorizing artifact patterns. This design bridges generative modeling and pixel-level localization, achieving a better balance between interpretability, robustness, and generalization.

3. Methodology

3.1. Motivation

Image forgery detection faces a fundamental challenge: forged regions are open-world and endlessly diverse, while real images follow a stable and compact distribution. Learning “what fake looks like” does not scale with the prolifera-

tion of manipulation types. We argue that a more principled strategy is to model *realness* instead of forgery.

A Masked Autoencoder (MAE), pretrained on large-scale natural images, implicitly captures this realness prior [16, 38]. It reconstructs authentic content with high fidelity but consistently fails on manipulated regions that deviate from the natural image manifold. Such reconstruction asymmetry provides an intrinsic and generalizable signal: if a model knows what is real, whatever it cannot faithfully reconstruct must be suspicious.

However, MAE reconstruction alone yields only coarse discrepancies, offering limited guidance for precise localization. What is missing is a mechanism that can iteratively refine and amplify these weak signals. This motivates a task-adaptive closed loop in which initial anomaly cues guide subsequent reconstruction, enabling the system to progressively highlight regions inconsistent with the realness prior.

Based on this perspective, we design the Iterative Forgery Amplifier Network (IFA-Net) to operationalize a “Detect–Guide–Amplify” paradigm: *Detect* deviations from realness, *Guide* the generative prior using task cues, and *Amplify* the anomaly response. This shift from learning forgery patterns to leveraging reconstruction-based realness allows the model to generalize effectively to unseen manipulation types, as it no longer depends on manipulation-specific cues.

A recent work in face forgery detection leverages an end-to-end reconstruction-classification framework [3], which

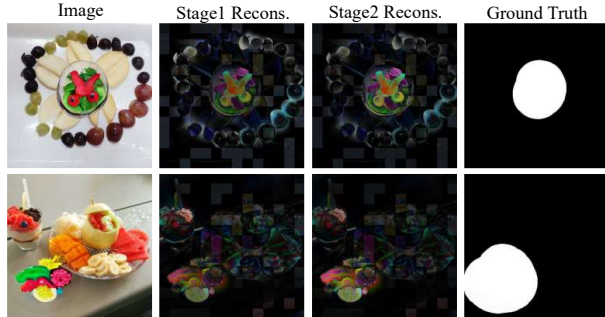


Figure 3. Visualization of anomaly amplification. We compare reconstructed images and residual maps from Stage 1 and Stage 2. In Stage 1, the frozen MAE can already produce coarse forgery cues—although weak and noisy, they indicate that the MAE indeed encodes a realness prior. In Stage 2, prompt-guided reconstruction forces the model to fail more strongly on forged regions, further amplifying these forgery cues and yielding a much cleaner and more salient residual map that better supports the final segmentation.

aligns with our strategy of using reconstruction to identify suspicious regions.

3.2. Realness-Guided Closed-Loop Detection

As illustrated in Fig. 2, IFA-Net consists of two collaborative stages that share a Dual-Stream Segmentation Network (DSSN), forming a “Detect–Guide–Amplify” task-adaptive closed loop grounded in a frozen MAE.

In the first stage, the frozen MAE performs an unconditional reconstruction of the input image and produces an initial reconstruction residual. This residual encodes deviations from the natural image manifold and is fused with the original image by the DSSN to produce a coarse forgery mask. This stage thus focuses on *Anomaly Discovery*, exposing subtle manifold discrepancies without task-specific guidance.

In the second stage, the coarse mask is treated as an explicit structural prior and is converted into task-dependent prompts via a lightweight Prompt Encoder. These prompts are injected into the frozen MAE encoder through a FiLM-based modulation layer inside the proposed Task-Adaptive Prior Injection (TAPI) module. The modulated encoder features are then fed into a trainable decoder, which is encouraged to *fail more strongly* on suspicious regions during reconstruction. The resulting residual, being significantly amplified in forged areas and suppressed in authentic regions, is again processed by the shared DSSN to refine the segmentation mask.

In this way, Stage I performs anomaly discovery using a universal reconstruction prior, while Stage II performs guided anomaly amplification by steering the generative prior toward suspicious regions. The two stages

are jointly optimized, forming an explicit closed loop between generative modeling (realness prior) and discriminative segmentation (pixel-level localization), and yielding interpretable and robust forgery localization. In recent works, visual prompting has been used to guide segmentation tasks, such as in explicit visual prompting [21] for foreground segmentation.

3.3. Dual-Stream Segmentation Network (DSSN)

We now detail the Dual-Stream Segmentation Network (DSSN), which is shared across both stages. The DSSN is designed to jointly capture high-level semantic structure and low-level artifact cues, enabling precise discrimination between authentic and manipulated regions.

Compared with the original SegFormer [41], DSSN incorporates dual inputs (the original image and an MAE residual map) and introduces cross-stream fusion atop dual encoders. This design is inspired by multi-source manipulation localization networks such as CFL-Net [27] and MFNet [31], which demonstrate the benefit of contrastive multi-branch cues.

3.3.1. Encoder Structure

The input image $\mathbf{X} \in \mathbb{R}^{H \times W \times C}$ and a residual map $\mathbf{X}_{\text{rec}} \in \mathbb{R}^{H \times W \times C}$ are fed into a content stream and an artifact stream, respectively, where H and W denote the spatial resolution and C denotes the number of channels. The content stream focuses on high-level semantics and scene structure, while the artifact stream focuses on fine-grained inconsistencies highlighted by the MAE residual.

Each stream applies an overlapped patch embedding module followed by a hierarchical transformer backbone, producing multi-scale features at a fixed number of stages. The content and artifact features at stage ℓ are denoted as $\mathbf{F}_{\text{con}}^{\ell} \in \mathbb{R}^{B \times N_{\ell} \times D_{\ell}}$ and $\mathbf{F}_{\text{art}}^{\ell} \in \mathbb{R}^{B \times N_{\ell} \times D_{\ell}}$, where B is the batch size, N_{ℓ} is the number of tokens and D_{ℓ} is the channel dimension at stage ℓ .

To enable interaction between semantic and artifact information, we apply cross-stream fusion via multi-head cross-attention at each stage. Specifically, the content features act as queries and the artifact features act as keys and values:

$$\tilde{\mathbf{F}}_{\text{con}}^{\ell} = \text{CrossAttn}(\mathbf{F}_{\text{con}}^{\ell}, \mathbf{F}_{\text{art}}^{\ell}, \mathbf{F}_{\text{art}}^{\ell}), \quad (1)$$

where $\text{CrossAttn}(\mathbf{Q}, \mathbf{K}, \mathbf{V})$ denotes multi-head cross-attention with queries \mathbf{Q} , keys \mathbf{K} , and values \mathbf{V} . This design allows semantic tokens to attend to artifact cues, progressively integrating manifold discrepancy information into the semantic representation. The fused content features at each stage, denoted by $\tilde{\mathbf{F}}_{\text{con}}^{\ell}$, form a complementary multi-scale representation that captures both global context and local inconsistencies.

3.3.2. Decoder and Output

The DSSN decoder aggregates the multi-scale fused features $\tilde{\mathbf{F}}_{\text{con}}^\ell$ into a dense prediction map. Concretely, all stages are first projected to a unified channel dimension and then upsampled to a common spatial resolution. These feature maps are concatenated along the channel dimension, compressed via a linear projection, and finally upsampled to the original image resolution to produce a single-channel forgery probability map. A Sigmoid activation is applied to convert this map into a pixel-wise probability mask.

The same decoder (and encoder weights) are shared between Stage I and Stage II. This weight sharing enforces consistent feature usage across coarse and refined predictions, reduces the parameter count, and stabilizes the closed-loop training process.

3.4. Task-Adaptive Prior Injection (TAPI)

The core mechanism of IFA-Net lies in constructing a two-stage closed loop based on the MAE realness prior [16], dynamically coupling generative reconstruction and discriminative segmentation. The proposed Task-Adaptive Prior Injection (TAPI) module implements the ‘‘Guide–Amplify’’ steps by converting coarse masks into prompts and using them to modulate MAE encoder features.

The frozen MAE encoder $E_{\text{MAE}}(\cdot)$ and the trainable decoder used in Stage II $D_{\text{MAE}}(\cdot)$ form the generative backbone. Given an input image \mathbf{X} , the encoder produces a token sequence $\mathbf{Z} \in \mathbb{R}^{B \times N \times D}$, where N is the number of patches and D is the token dimension. TAPI uses the coarse mask from Stage I to generate task-dependent prompts and then modulates \mathbf{Z} via FiLM to guide the subsequent reconstruction.

3.4.1. Prompt Encoding

The coarse mask predicted by Stage I, denoted as $\mathbf{M}_{\text{crs}} \in \mathbb{R}^{B \times H \times W}$, is converted by the Prompt Encoder into a compact set of task-adaptive tokens $\mathbf{T} \in \mathbb{R}^{B \times N_p \times D_p}$, where N_p is the number of prompt tokens and D_p is the prompt embedding dimension.

Internally, the Prompt Encoder first reduces the spatial resolution of \mathbf{M}_{crs} through a stack of convolutional layers with downsampling, producing a feature map of size $B \times C_p \times H_p \times W_p$, where H_p and W_p are lower than H and W by a fixed factor and C_p denotes the intermediate channel dimension. This feature map is then reshaped into B sequences of length $N_p = H_p W_p$ and linearly projected to dimension D_p , yielding the prompt token matrix \mathbf{T} . These tokens summarize the spatial distribution and shape of suspicious regions and will be used to generate FiLM parameters.

3.4.2. Guided Reconstruction via FiLM

To inject task information into the MAE encoder features, we adopt Feature-wise Linear Modulation (FiLM). From

the prompt tokens \mathbf{T} , we first obtain a global summary vector by applying average pooling along the token dimension. Two lightweight parametric mappings then transform this summary vector into scaling and shifting coefficients $\gamma \in \mathbb{R}^{B \times D}$ and $\beta \in \mathbb{R}^{B \times D}$, respectively. These coefficients are broadcast along the token dimension and applied to the encoder tokens \mathbf{Z} in a feature-wise affine transformation:

$$\tilde{\mathbf{Z}} = \gamma \odot \mathbf{Z} + \beta, \quad (2)$$

where \odot denotes element-wise multiplication with broadcasting.

The modulated encoder tokens $\tilde{\mathbf{Z}}$ are passed to the trainable decoder $D_{\text{MAE}}(\cdot)$, which produces a guided reconstructed image and its corresponding residual. Importantly, the MAE encoder $E_{\text{MAE}}(\cdot)$ remains frozen in both stages, preserving a stable realness prior, while only $D_{\text{MAE}}(\cdot)$ is fine-tuned in Stage II to respond to the FiLM modulation. This design encourages the decoder to systematically alter its reconstruction strategy in regions flagged by the prompts, effectively forcing stronger reconstruction failures on forged areas and yielding an amplified, more structured residual map (see Fig. 3).

3.5. Loss Function

IFA-Net jointly optimizes two segmentation branches in an end-to-end manner to ensure stable coarse localization and accurate refined detection. The input image is denoted as \mathbf{X} and the corresponding ground-truth mask is denoted as \mathbf{M}^* . The loss of the first stage is defined as the combination of Binary Cross-Entropy (BCE) and Dice loss [34]:

$$\mathcal{L}_{\text{crs}} = \mathcal{L}_{\text{BCE}}(\mathbf{M}_{\text{crs}}, \mathbf{M}^*) + \mathcal{L}_{\text{Dice}}(\mathbf{M}_{\text{crs}}, \mathbf{M}^*), \quad (3)$$

where \mathbf{M}_{crs} denotes the coarse mask predicted by Stage I. This term enforces reliable anomaly discovery and provides a stable guidance signal for the following refinement stage.

The refinement-stage loss for Stage II is formulated in the same way:

$$\mathcal{L}_{\text{ref}} = \mathcal{L}_{\text{BCE}}(\mathbf{M}_{\text{ref}}, \mathbf{M}^*) + \mathcal{L}_{\text{Dice}}(\mathbf{M}_{\text{ref}}, \mathbf{M}^*), \quad (4)$$

where \mathbf{M}_{ref} is the refined mask obtained after prior injection and anomaly amplification. It encourages precise pixel-level localization and sharper boundaries.

Finally, the overall training objective combines the two losses as

$$\mathcal{L}_{\text{total}} = \mathcal{L}_{\text{ref}} + \alpha \mathcal{L}_{\text{crs}}, \quad (5)$$

where the balancing coefficient α is set to 0.5, which controls the contribution of the coarse-stage supervision. A moderate weight stabilizes the training process while ensuring that the refined prediction dominates the final optimization.

Table 1. Quantitative results on GIT and TT benchmarks. Comparison of the proposed method with recent state-of-the-art approaches. Values are reported as IoU / F1. Best and second-best results for IoU and F1 are independently shown in **bold** and underline, respectively.

Dataset	TruFor		PSCC-Net		MVSS-Net		SPAN		IML-ViT		MaskCLIP		DcDsDiff		Ours	
	IoU	F1	IoU	F1	IoU	F1	IoU	F1	IoU	F1	IoU	F1	IoU	F1	IoU	F1
GIT Benchmarks																
OpenSDI	0.369	0.426	0.297	0.368	0.298	0.349	0.284	0.349	0.325	0.373	<u>0.427</u>	<u>0.494</u>	0.385	0.445	0.487	0.620
GIT10K	0.770	0.815	0.392	0.754	0.453	0.518	0.137	0.257	<u>0.882</u>	0.859	0.694	0.765	0.801	<u>0.864</u>	0.928	0.963
CocoGlide	0.481	0.552	0.769	0.869	0.419	0.533	0.276	0.411	0.291	0.440	0.783	0.878	<u>0.878</u>	<u>0.935</u>	0.887	0.940
Inpaint32K	0.711	0.762	0.116	0.207	0.496	0.578	0.456	0.541	0.703	<u>0.775</u>	0.390	0.480	<u>0.790</u>	0.852	0.811	0.896
AVG	0.583	0.639	0.394	0.550	0.416	0.494	0.288	0.390	0.550	0.612	0.573	0.654	<u>0.713</u>	<u>0.774</u>	0.778	0.855
TT Benchmarks																
IMD	0.552	<u>0.601</u>	0.276	0.437	0.331	0.393	0.153	0.264	<u>0.548</u>	0.619	0.541	0.569	0.396	0.568	0.392	0.563
NIST16	0.447	0.522	0.196	0.294	0.181	0.226	0.396	0.582	0.242	0.326	0.694	0.751	<u>0.843</u>	<u>0.915</u>	0.949	0.974
CASIA	<u>0.637</u>	<u>0.724</u>	0.295	0.442	0.284	0.427	0.137	0.170	0.675	0.806	0.594	0.625	<u>0.637</u>	0.713	0.416	0.587
AVG	0.545	0.616	0.256	0.391	0.265	0.349	0.229	0.338	0.488	0.584	<u>0.610</u>	0.648	0.625	0.732	0.586	<u>0.708</u>

4. Experiments and Results

4.1. Experimental Setup

Datasets. We evaluate IFA-Net across seven public benchmarks spanning both diffusion-based and GAN-based Generative Image Tampering (GIT) and Traditional Tampering (TT) scenarios. To ensure consistent input across all settings, all images are resized to 512×512 .

These benchmarks collectively cover a wide range of manipulation types. For Generative Image Tampering, 1) *OpenSDID* [39] provides diverse inpainting prompts and mask shapes for modeling diffusion-aware inconsistencies; 2) *GIT10K* [15] contains 10,000 authentic–forged pairs with varying mask scales and editing operations; 3) *CocoGlide* [20, 26] derives high-fidelity semantic inpainting samples from COCO using Glide and Stable Diffusion; and 4) *Inpaint32K* [37] includes restorations produced by diffusion, GAN, and CNN-based inpainting models with diverse masks, enabling cross-mask generalization testing. For Traditional Tampering, 5) *IMD2020* [28] contains 2,010 manipulated images covering common splicing and copy–move cases; 6) *NIST16* [12] provides high-resolution forgeries for device- and compression-robustness evaluation; and 7) *CASIA* [10] serves as a classical large-scale benchmark for traditional manipulation localization.

We first pretrain our model on the training split of OpenSDID, which contains images generated by Stable Diffusion 1.5. The pretrained weights are then used for dataset-specific fine-tuning and evaluation on other benchmarks. This training strategy enables the model to learn general diffusion-aware priors while allowing fair cross-dataset comparison.

Baselines. We compare against a comprehensive set of state-of-the-art methods covering both traditional tampering localization and diffusion-based editing forensics. Conventional baselines include TruFor [13], PSCC-Net [23], MVSS-Net [8], and SPAN [17]. For generative-editing scenarios, we benchmark against Transformer- and diffusion-

driven methods such as IML-ViT [25], MaskCLIP [11], and DcDsDiff [15]. This collection spans pixel-level, multi-scale, frequency-guided, and reconstruction-based paradigms.

Evaluation Metrics. Following common practice, we report *F1-score* and *Intersection-over-Union (IoU)*. F1 reflects the trade-off between precision and recall, indicating the overall detection capability, while IoU quantifies the spatial overlap between the predicted and ground-truth masks, highlighting localization accuracy.

Implementation Details. IFA-Net is implemented in PyTorch and trained with Distributed Data Parallel (DDP) on eight NVIDIA RTX 4090 GPUs. The MAE backbone uses ViT-Large weights pretrained on ImageNet-1k, and the dual-stream segmentation network adopts MiT-B2 weights pretrained on ADE20K. Training is performed for up to 100 epochs with an effective batch size of 32 using AdamW (initial learning rate $2e-5$, weight decay $1e-5$). An early-stopping criterion based on validation IoU (patience 10 epochs) selects the final model.

4.2. State-of-the-Art Comparison

We now compare our method with recent state-of-the-art approaches on both generative-editing (GIT) and traditional tampering (TT) benchmarks to comprehensively evaluate its effectiveness and generalization.

Results on GIT Benchmarks. Table 1 compares IFA-Net with existing state-of-the-art detectors across four generative-editing benchmarks—*OpenSDID*, *GIT10K*, *CocoGlide*, and *Inpaint32K*. IFA-Net consistently achieves the best or second-best performance on all datasets, reaching an average IoU of 0.778 and F1 of 0.855, establishing a new state of the art for generative forgery localization.

On *OpenSDID*, where our model is pretrained, IFA-Net achieves an IoU of 0.487 and F1 of 0.620, demonstrating the effectiveness of our realism-driven paradigm. More importantly, the model exhibits strong cross-dataset general-

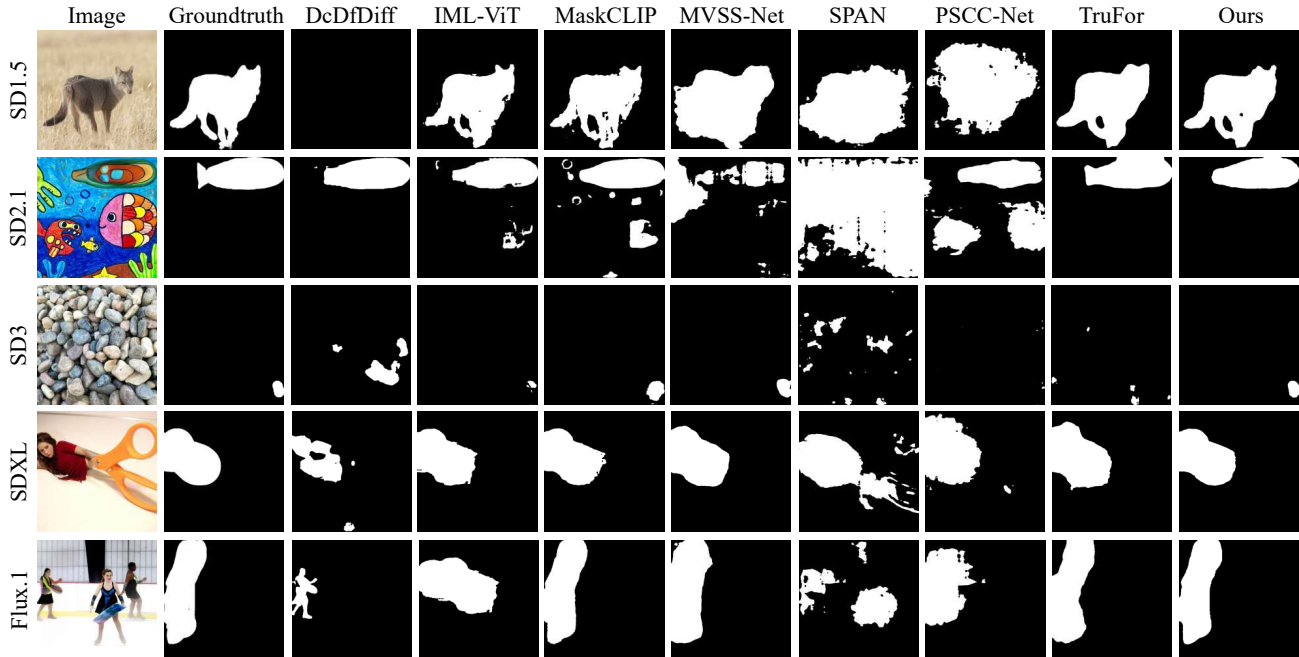


Figure 4. Qualitative comparison on OpenSDID. Examples are selected from five diffusion generators (SD1.5, SD2.1, SD3, SDXL, and Flux.1). IFA-Net produces cleaner and more accurate localization masks that align closely with the ground truth, whereas other methods often yield incomplete or fragmented detections.

Table 2. Ablation study of IFA-Net. Performance impact of each component on diffusion-based (GIT-AVG) and traditional tampering (TT-AVG) benchmarks. Index I represents a single-stream baseline that concatenates the original image and residual map as input. AD denotes the Adaptive Decoder. Best results are highlighted in **bold**.

Index	Components			GIT-AVG		TT-AVG	
	DSSN	TAPI	AD	IoU	F1	IoU	F1
I	✗	✗	✗	0.670	0.770	0.459	0.608
II	✓	✗	✗	0.684	0.782	0.483	0.625
III	✓	✓	✗	0.745	0.823	0.554	0.670
IV	✓	✓	✓	0.778	0.855	0.586	0.708

ization: on *GIT10K*, *CocoGlide*, and *Inpaint32K*, IFA-Net maintains superior or highly competitive performance, indicating robust transferability across diverse diffusion models, prompt conditions, and mask complexities. This cross-dataset stability demonstrates that modeling authenticity via a frozen MAE prior—rather than memorizing dataset-specific artifact patterns—enables the network to capture generalizable deviations from the natural image manifold.

Beyond quantitative metrics, our approach also improves interpretability. By grounding detection in the reconstruction behavior of a real-image prior, IFA-Net provides explicit visual cues corresponding to physical inconsistencies, making predicted masks more semantically meaningful for

forensic applications.

Results on TT Benchmarks. Although primarily designed for diffusion-based forgeries, IFA-Net generalizes well to conventional tampering datasets including *IMD2020*, *NIST16*, and *CASIA*, which involve copy-move, splicing, and region removal operations.

As shown in Table 1, IFA-Net achieves an average F1 of 0.708, comparable to DcDsDiff and outperforming most classical detectors. This demonstrates that the learned realness prior from large-scale authentic imagery generalizes beyond diffusion or semantic editing, enabling IFA-Net to capture structural and texture inconsistencies inherent to traditional tampering. In particular, the frozen MAE prior preserves natural statistical dependencies, allowing our model to identify subtle copy-move traces and splicing boundaries that often confuse purely discriminative methods.

Qualitative Comparisons. Figure 4 presents qualitative results on the *OpenSDID* dataset. Across five diffusion generators—SD1.5, SD2.1, SD3, SDXL, and Flux.1—IFA-Net produces cleaner and more coherent localization masks that align closely with the ground truth. Predicted boundaries are sharper and more complete, showing the model’s ability to suppress background noise and to highlight fine-grained diffusion traces or small edited objects. This qualitative consistency supports our claim that the proposed closed-loop amplification not only enhances numerical per-

formance but also yields visually interpretable evidence.

4.3. Ablation Study

To assess the individual and combined contributions of each component in IFA-Net, we conduct a comprehensive ablation study on both diffusion-based (GIT-AVG) and traditional tampering (TT-AVG) benchmarks. Starting from a single-stream baseline, we progressively introduce the Dual-Stream Segmentation Network (DSSN), the Task-Adaptive Prior Injection module (TAPI), and the Adaptive Decoder (AD).

Table 2 presents the quantitative results. The baseline configuration (Index I) achieves 0.670 IoU and 0.770 F1 on GIT-AVG, and 0.459 IoU and 0.608 F1 on TT-AVG. This limited performance stems from the model’s inability to separately process semantic content and artifact residuals. Introducing the DSSN (Index II) brings moderate improvements of 1.4% IoU and 1.2% F1 on GIT-AVG, and 2.4% IoU and 1.7% F1 on TT-AVG, attributed to its dual-encoder architecture that decouples semantic and artifact cues.

Adding the TAPI module (Index III) yields the most substantial boost, with 6.1% IoU and 4.1% F1 improvements on GIT-AVG, and 7.1% IoU and 4.5% F1 on TT-AVG compared to DSSN alone. This validates that task-adaptive guidance is essential for anomaly amplification. The TAPI module converts coarse predictions into structural prompts and injects them via FiLM-based modulation, steering reconstruction to emphasize manifold deviations. The Adaptive Decoder (Index IV) further refines boundary precision, providing additional gains of 3.3% IoU and 3.2% F1 on GIT-AVG, and 3.2% IoU and 3.8% F1 on TT-AVG. Overall, the complete IFA-Net surpasses the baseline by 10.8% IoU and 8.5% F1 on GIT-AVG, and 12.7% IoU and 10.0% F1 on TT-AVG, demonstrating strong synergy among all components.

4.4. Robustness Evaluation

To assess the stability of IFA-Net under common post-processing distortions, we evaluate its robustness against Jpeg compression and Gaussian blur on both diffusion-based (GIT) and traditional tampering (TT) benchmarks. Figure 5 reports the average F1-scores under increasing distortion levels.

Under Jpeg compression in the GIT domain, IFA-Net maintains the highest F1-scores at high quality levels (100-80), benefiting from task-adaptive prior injection that emphasizes manifold discrepancy rather than compression-sensitive artifacts. As compression quality decreases to 60 and 50, the performance gap narrows with MaskCLIP and DcDsDiff, though IFA-Net remains competitive. For Gaussian blur perturbations in the GIT domain, our method achieves strong F1-scores at lower blur levels (0-11), outperforming most baselines. However, as blur intensity

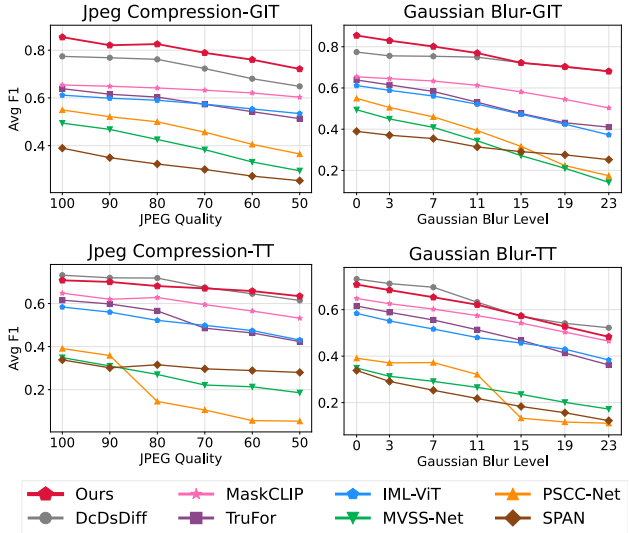


Figure 5. Robustness analysis under Gaussian blur and Jpeg compression.

increases beyond level 15, DcDsDiff exhibits better resilience. The diffusion-prior-based reconstruction preserves global structural cues more effectively under severe smoothing conditions.

In the TT domain, IFA-Net outperforms conventional detectors under Jpeg compression at high qualities (100-80), while DcDsDiff shows stronger resilience under severe compression (60-50). The reconstruction-based framework in DcDsDiff maintains better stability when handling quantization artifacts introduced by aggressive compression. For Gaussian blur, IFA-Net shows competitive performance at moderate blur levels (0-11), but DcDsDiff demonstrates superior stability at higher blur levels. The global reconstruction framework in DcDsDiff is less affected by texture smoothing compared to our manifold-based residual amplification approach. Despite these limitations under extreme perturbations, IFA-Net consistently surpasses PSCC-Net, MVSS-Net, and SPAN across most distortion levels, validating that the closed-loop amplification provides a resilient foundation for practical forensic scenarios.

5. Conclusion

We presented IFA-Net, a realism-driven framework for forgery localization. Instead of learning forgery patterns, IFA-Net models authenticity by exploiting the reconstruction asymmetry of a frozen MAE trained on real images. Through a two-stage closed-loop design—*anomaly discovery and anomaly amplification*—the model converts reconstruction residuals into explicit localization cues. This enables the network to learn *what is real* rather than memorize *what is fake*, achieving robust and explainable performance

across diverse manipulations. Experiments confirm its superiority under perturbations such as compression and blur. Future work will extend this paradigm to video and multi-modal forensics, and explore weakly supervised optimization toward a unified, realness-centric forensic framework.

References

- [1] Vishal Asnani, Xi Yin, Tal Hassner, Sijia Liu, and Xiaoming Liu. Proactive image manipulation detection. In *IEEE/CVF Conference on Computer Vision and Pattern Recognition (CVPR)*, pages 15365–15374, 2022.
- [2] Vishal Asnani, Xi Yin, Tal Hassner, and Xiaoming Liu. Malp: Manipulation localization using a proactive scheme. In *IEEE/CVF Conference on Computer Vision and Pattern Recognition (CVPR)*, pages 12343–12352, 2023.
- [3] Junyi Cao, Chao Ma, Taiping Yao, Shen Chen, Shouhong Ding, and Xiaokang Yang. End-to-end reconstruction-classification learning for face forgery detection. In *IEEE/CVF Conference on Computer Vision and Pattern Recognition (CVPR)*, pages 4103–4112. IEEE, 2022.
- [4] George Cazenavette, Avneesh Sud, Thomas Leung, and Ben Usman. Fakeinversion: Learning to detect images from unseen text-to-image models by inverting stable diffusion. In *IEEE/CVF Conference on Computer Vision and Pattern Recognition (CVPR)*, pages 10759–10769, 2024.
- [5] Baoying Chen, Jishen Zeng, Jianquan Yang, and Rui Yang. Drcr: Diffusion reconstruction contrastive training towards universal detection of diffusion generated images. In *International Conference on Machine Learning (ICML)*, 2024.
- [6] Beilin Chu, Xuan Xu, Xin Wang, Yufei Zhang, Weiwei You, and Linna Zhou. Fire: Robust detection of diffusion-generated images via frequency-guided reconstruction error. In *IEEE/CVF Conference on Computer Vision and Pattern Recognition (CVPR)*, pages 12830–12839. IEEE, 2025.
- [7] Davide Cozzolino and Luisa Verdoliva. Noiseprint: A cnn-based camera model fingerprint. *IEEE Transactions on Information Forensics and Security (TIFS)*, 15:144–159, 2020.
- [8] Chengbo Dong, Xinru Chen, Ruohan Hu, Juan Cao, and Xirong Li. Mvss-net: Multi-view multi-scale supervised networks for image manipulation detection. *IEEE Transactions on Pattern Analysis and Machine Intelligence (TPAMI)*, 45(3):3539–3553, 2023.
- [9] Cheng Dong, Jiantao Liu, Jieming Zhu, Xudong Sun, and Yongjian Xu. Mvss-net: Multi-view multi-scale supervision network for image manipulation detection. *IEEE Transactions on Pattern Analysis and Machine Intelligence (TPAMI)*, 45(3):3348–3363, 2023.
- [10] Jing Dong, Wei Wang, and Tieniu Tan. Casia image tampering detection evaluation database. In *IEEE China Summit and International Conference on Signal and Information Processing (ChinaSIP)*, pages 422–426. IEEE, 2013.
- [11] Xiaoyi Dong, Jianmin Bao, Yinglin Zheng, Ting Zhang, Dongdong Chen, Hao Yang, Ming Zeng, Weiming Zhang, Lu Yuan, Dong Chen, Fang Wen, and Nenghai Yu. Maskclip: Masked self-distillation advances contrastive language-image pretraining. In *IEEE/CVF Conference on Computer Vision and Pattern Recognition (CVPR)*, pages 10995–11005. IEEE, 2023.
- [12] Haiying Guan, Mark Kozak, Eric Robertson, Yooyoung Lee, Amy N. Yates, Andrew Delgado, Daniel Zhou, Timothée Kheyrkhan, Jeff Smith, and Jonathan G. Fiscus. Mfc datasets: Large-scale benchmark datasets for media forensic challenge evaluation. In *Proc. IEEE Winter Conf. Appl. Comput. Vis. Workshops (WACVW)*, pages 63–72, 2019.
- [13] Fabrizio Guillaro, Davide Cozzolino, Avneesh Sud, Nicholas Dufour, and Luisa Verdoliva. Trufor: Leveraging all-round clues for trustworthy image forgery detection and localization. In *IEEE/CVF Conference on Computer Vision and Pattern Recognition (CVPR)*, pages 20606–20615. IEEE, 2023.
- [14] Xiao Guo, Xiaohong Liu, Zhiyuan Ren, Steven Grosz, Iacopo Masi, and Xiaoming Liu. Hierarchical fine-grained image forgery detection and localization. In *IEEE/CVF Conference on Computer Vision and Pattern Recognition (CVPR)*, pages 3155–3165, 2023.
- [15] Qixian Hao, Shaozhang Niu, Jiwei Zhang, and Kai Wang. Dcddiff: Dual-conditional and dual-stream diffusion model for generative image tampering localization. In *Proceedings of the Thirty-Fourth International Joint Conference on Artificial Intelligence (IJCAI)*, pages 1071–1079. ijcai.org, 2025.
- [16] Kaiming He, Xinlei Chen, Saining Xie, Yanghao Li, Piotr Dollár, and Ross B. Girshick. Masked autoencoders are scalable vision learners. In *IEEE/CVF Conference on Computer Vision and Pattern Recognition (CVPR)*, pages 15979–15988. IEEE, 2022.
- [17] Xuefeng Hu, Zhihan Zhang, Zhenye Jiang, Syomantak Chaudhuri, Zhenheng Yang, and Ram Nevatia. Span: Spatial pyramid attention network for image manipulation localization. In *Computer Vision - ECCV 2020 - 16th European Conference*, pages 312–328. Springer, 2020.
- [18] Dong Li, Jiaying Zhu, Xueyang Fu, Xun Guo, Yidi Liu, Gang Yang, Jiawei Liu, and Zheng-Jun Zha. Noise-assisted prompt learning for image forgery detection and localization. In *European Conference on Computer Vision (ECCV)*, pages 18–36, 2024.
- [19] Shuai-bo Li, Wei Ma, Jianwei Guo, Shibiao Xu, Benchong Li, and Xiaopeng Zhang. Unionformer: Unified-learning transformer with multi-view representation for image manipulation detection and localization. In *IEEE/CVF Conference on Computer Vision and Pattern Recognition (CVPR)*, pages 12523–12533, 2024.
- [20] Tsung-Yi Lin, Michael Maire, Serge J. Belongie, James Hays, Pietro Perona, Deva Ramanan, Piotr Dollár, and C. Lawrence Zitnick. Microsoft coco: Common objects in context. In *Computer Vision - ECCV 2014 - 13th European Conference*, pages 740–755. Springer, 2014.
- [21] Weihuang Liu, Xi Shen, Chi-Man Pun, and Xiaodong Cun. Explicit visual prompting for universal foreground segmentations. *CoRR*, abs/2305.18476, 2023.
- [22] Weihuang Liu, Xi Shen, Chi-Man Pun, and Xiaodong Cun. Explicit visual prompting for low-level structure segmentations. In *IEEE/CVF Conference on Computer Vision and Pattern Recognition (CVPR)*, pages 19434–19445, 2023.
- [23] Xiaohong Liu, Yaojie Liu, Jun Chen, and Xiaoming Liu. Pscn-net: Progressive spatio-channel correlation network for

- image manipulation detection and localization. *IEEE Transactions on Circuits and Systems for Video Technology*, 32(11):7505–7517, 2022.
- [24] Yunpeng Luo, Junlong Du, Ke Yan, and Shouhong Ding. Lare²: Latent reconstruction error based method for diffusion-generated image detection. *arXiv preprint arXiv:2403.17465*, 2024.
- [25] Xiaochen Ma, Bo Du, Zhuohang Jiang, Ahmed Y Al Hammadi, and Jizhe Zhou. Iml-vit: Benchmarking image manipulation localization by vision transformer. *arXiv preprint arXiv:2307.14863*, 2023.
- [26] Alexander Quinn Nichol, Prafulla Dhariwal, Aditya Ramesh, Pranav Shyam, Pamela Mishkin, Bob McGrew, Ilya Sutskever, and Mark Chen. Glide: Towards photorealistic image generation and editing with text-guided diffusion models. In *International Conference on Machine Learning (ICML)*, pages 16784–16804. PMLR, 2022.
- [27] Fahim Faisal Niloy, Kishor Kumar Bhaumik, and Simon S. Woo. Cfl-net: Image forgery localization using contrastive learning. In *IEEE/CVF Winter Conference on Applications of Computer Vision (WACV)*, pages 4631–4640, 2023.
- [28] Adam Novozámský, Babak Mahdian, and Stanislav Saic. Imd2020: A large-scale annotated dataset tailored for detecting manipulated images. In *IEEE Winter Applications of Computer Vision Workshops (WACV)*, pages 71–80. IEEE, 2020.
- [29] Utkarsh Ojha, Yuheng Li, and Yong Jae Lee. Towards universal fake image detectors that generalize across generative models. In *IEEE/CVF Conference on Computer Vision and Pattern Recognition (CVPR)*, pages 24480–24489, 2023.
- [30] Dustin Podell, Zion English, Kyle Lacey, Andreas Blattmann, Tim Dockhorn, Jonas Müller, Joe Penna, and Robin Rombach. Sdxl: Improving latent diffusion models for high-resolution image synthesis. In *International Conference on Learning Representations (ICLR)*, 2024.
- [31] Ruyong Ren, Qixian Hao, Shaozhang Niu, Keyang Xiong, Jiwei Zhang, and Maosen Wang. Mfi-net: Multi-feature fusion identification networks for artificial intelligence manipulation. *IEEE Transactions on Circuits and Systems for Video Technology*, 34(2):1266–1280, 2024.
- [32] Jonas Ricker, Denis Lukovnikov, and Asja Fischer. Aeroblade: Training-free detection of latent diffusion images using autoencoder reconstruction error. In *IEEE/CVF Conference on Computer Vision and Pattern Recognition (CVPR)*, pages 9130–9140. IEEE, 2024.
- [33] Robin Rombach, Andreas Blattmann, Dominik Lorenz, Patrick Esser, and Björn Ommer. High-resolution image synthesis with latent diffusion models. In *IEEE/CVF Conference on Computer Vision and Pattern Recognition (CVPR)*, pages 10674–10685, 2022.
- [34] Olaf Ronneberger, Philipp Fischer, and Thomas Brox. U-net: Convolutional networks for biomedical image segmentation. In *Medical Image Computing and Computer-Assisted Intervention - MICCAI 2015*, pages 234–241. Springer, 2015.
- [35] Nataniel Ruiz, Yuanzhen Li, Varun Jampani, Yael Pritch, Michael Rubinstein, and Kfir Aberman. Dreambooth: Fine tuning text-to-image diffusion models for subject-driven generation. In *IEEE/CVF Conference on Computer Vision and Pattern Recognition (CVPR)*, pages 22500–22510, 2023.
- [36] Chitwan Saharia, William Chan, Saurabh Saxena, Lala Li, Jay Whang, Emily L. Denton, Seyed Kamyar Seyed Ghasemipour, Raphael Gontijo Lopes, Burcu Karagol Ayan, Tim Salimans, Jonathan Ho, David J. Fleet, and Mohammad Norouzi. Photorealistic text-to-image diffusion models with deep language understanding. In *Advances in Neural Information Processing Systems (NeurIPS)*, 2022.
- [37] Kai Wang, Shaozhang Niu, Qixian Hao, and Jiwei Zhang. Inpdiffusion: Image inpainting localization via conditional diffusion models. In *AAAI Conference on Artificial Intelligence (AAAI)*, pages 7771–7779. AAAI Press, 2025.
- [38] Yi Wang, Hugo Hernández Hernández, Conrad M. Albrecht, and Xiao Xiang Zhu. Feature guided masked autoencoder for self-supervised learning in remote sensing. *IEEE Journal of Selected Topics in Applied Earth Observations and Remote Sensing*, 18:321–336, 2025.
- [39] Yabin Wang, Zhiwu Huang, and Xiaopeng Hong. Opensdi: Spotting diffusion-generated images in the open world. In *IEEE/CVF Conference on Computer Vision and Pattern Recognition (CVPR)*, pages 4291–4301. Computer Vision Foundation / IEEE, 2025.
- [40] Zhendong Wang, Jianmin Bao, Wengang Zhou, Weilun Wang, Hezhen Hu, Hong Chen, and Houqiang Li. Dire for diffusion-generated image detection. In *IEEE/CVF International Conference on Computer Vision (ICCV)*, pages 22388–22398, 2023.
- [41] Enze Xie, Wenhai Wang, Zhiding Yu, Anima Anandkumar, José M. Álvarez, and Ping Luo. Segformer: Simple and efficient design for semantic segmentation with transformers. In *Advances in Neural Information Processing Systems (NeurIPS)*, pages 12077–12090, 2021.
- [42] Zeqin Yu, Jiangqun Ni, Yuzhen Lin, Haoyi Deng, and Bin Li. Difforensics: Leveraging diffusion prior to image forgery detection and localization. In *IEEE/CVF Conference on Computer Vision and Pattern Recognition (CVPR)*, pages 12765–12774, 2024.
- [43] Xuanyu Zhang, Runyi Li, Jiwen Yu, Youmin Xu, Weiqi Li, and Jian Zhang. Editguard: Versatile image watermarking for tamper localization and copyright protection. In *IEEE/CVF Conference on Computer Vision and Pattern Recognition (CVPR)*, pages 11964–11974. IEEE, 2024.
- [44] Zhenfei Zhang, Mingyang Li, Xin Li, Ming-Ching Chang, and Jun-Wei Hsieh. Image manipulation detection with implicit neural representation and limited supervision. In *European Conference on Computer Vision (ECCV)*, pages 255–273, 2024.
- [45] Ziyin Zhou, Yunpeng Luo, Yuanchen Wu, Ke Sun, Jiayi Ji, Ke Yan, Shouhong Ding, Xiaoshuai Sun, Yunsheng Wu, and Rongrong Ji. Aigi-holmes: Towards explainable and generalizable ai-generated image detection via multimodal large language models. *arXiv preprint arXiv:2507.02664*, 2025.
- [46] Mingjian Zhu, Hanting Chen, Qiangyu Yan, Xudong Huang, Guanyu Lin, Wei Li, Zhijun Tu, Hailin Hu, Jie Hu, and Yunhe Wang. Genimage: A million-scale benchmark for detecting ai-generated image. In *Advances in Neural Information Processing Systems (NeurIPS)*, 2023.